IMPERIAL

Reconfigurable Intelligent Surfaces:
Beamforming, Modulation, and Channel Shaping

Yang Zhao

Supervisor: Prof. Bruno Clerckx

Department of Electrical and Electronic Engineering
Imperial College London

This dissertation is submitted for the degree of
Doctor of Philosophy

CSP Group March 2024

Declaration

I hereby declare that the contents presented in this dissertation are original and have been carried out by myself under the guidance of my supervisor Prof. Bruno Clerckx. Any work from other researchers, scholars, or sources have been properly cited and acknowledged. The contents have not been submitted in whole or in part for consideration of any other degree or qualification in any academic institution. I am aware of the ethical standards and academic integrity policies of Imperial College London, and I have adhered to these principles throughout the course of my study. In signing this declaration, I affirm my commitment to academic honesty, intellectual integrity, and the pursuit of knowledge in the service of truth and understanding.

The source code of all simulation results in this dissertation are publicly available at `https://github.com/snowztail/`.

Yang Zhao
March 2024

Abstract

This is where you write your abstract ...

Table of contents

List of figures

List of tables

Abbreviations

bpcu	bits per channel use
bps/Hz	bits per second per Hertz
AF	Amplify-and-Forward
AI	Artificial Intelligence
AM	Arithmetic Mean
AmBC	Ambient Backscatter Communication
AO	Alternating Optimization
AP	Access Point
AWGN	Additive White Gaussian Noise
BackCom	Backscatter Communication
BBC	Bistatic Backscatter Communication
BCD	Block Coordinate Descent
BD	Beyond-Diagonal
BER	Bit Error Rate
BIBO	Binary-Input Binary-Output
BLE	Bluetooth Low Energy
BLS	Backtracking Line Search
CLT	Central Limit Theorem
CP	Canonical Polyadic
CR	Cognitive Radio
CSCG	Circularly Symmetric Complex Gaussian
CSI	Channel State Information
CSIT	Channel State Information at the Transmitter
CW	Continuous Waveform

DC	Direct Current
DCMC	Discrete-input Continuous-output Memoryless Channel
DF	Decode-and-Forward
DMC	Discrete Memoryless Channel
DMMAC	Discrete Memoryless Multiple Access Channel
DMTC	Discrete Memoryless Thresholding Channel
DoF	Degree of Freedom
DP	Dynamic Programming
EIRP	Effective Isotropic Radiated Power
eMBB	enhanced Mobile Broadband
FDMA	Frequency-Division Multiple Access
FPGA	Field-Programmable Gate Array
GM	Geomtric Mean
GP	Geometric Programming
i.i.d.	independent and identically distributed
IC	Interference Channel
IM	Index Modulation
IoE	Internet of Everything
IoT	Internet of Things
KKT	Karush-Kuhn-Tucker
LC	Low-Complexity
LoRaWAN	Long Range Wide Area Network
LoS	Line-of-Sight
M2M	Machine-to-Machine
MAC	Multiple Access Channel
MBC	Monostatic Backscatter Communication
MC	Multiplication Coding
MIMO	Multiple-Input Multiple-Output
MISO	Multiple-Input Single-Output

ML	Maximum-Likelihood
MMSE	Minimum Mean-Square-Error
mMTC	massive Machine-Type Communication
MRC	Maximal Ratio Combining
MRT	Maximum Ratio Transmission
MSE	Mean-Square Error
NLoS	Non-Line-of-Sight
NOMA	Non-Orthogonal Multiple Access
OFDM	Orthogonal Frequency-Division Multiplexing
PAE	Power-Added Efficiency
PAPR	Peak-to-Average Power Ratio
PC	Point-to-point Channel
PDF	Probability Density Function
PGA	Projected Gradient Ascent
PIN	Positive Intrinsic Negative
PS	Power Splitting
PSK	Phase Shift Keying
QAM	Quadrature Amplitude Modulation
QoS	Quality of Service
R-E	Rate-Energy
RCG	Riemannian Conjugate Gradient
RF	Radio-Frequency
RFID	Radio-Frequency Identification
RIS	Reconfigurable Intelligent Surface
SC	Superposition Coding
SCA	Successive Convex Approximation
SDMA	Space-Division Multiple Access
SDP	Semi-Definite Programming
SDR	Semi-Definite Relaxation
SIC	Successive Interference Cancellation

SIMO	Single-Input Multiple-Output
SINR	Signal-to-Interference-plus-Noise Ratio
SISO	Single-Input Single-Output
SMAWK	Shor-Moran-Aggarwal-Wilber-Klawe
SMF	Scaled Matched Filter
SNR	Signal-to-Noise Ratio
SR	Symbiotic Radio
STAR	Simultaneous Transmission and Reflection
SVD	Singular Value Decomposition
SWIPT	Simultaneous Wireless Information and Power Transfer
TDMA	Time-Division Multiple Access
TS	Time Switching
UE	User Equipment
URLLC	Ultra-Reliable Low-Latency Communication
WF	Water-Filling
WIT	Wireless Information Transfer
WPCN	Wireless Powered Communication Network
WPT	Wireless Power Transfer
WSN	Wireless Sensor Network
WSR	Weighted Sum-Rate
ZF	Zero-Forcing

Notation

Constants

e	Euler's number $\simeq 2.71828\ldots$
$\jmath$	Imaginary unit $= \sqrt{-1}$
π	Archimedes' constant $\simeq 3.14159\ldots$

Objects

a, A	Scalar
$\mathbf{a}$	Column vector
$\mathbf{A}$	Matrix
$\mathcal{A}$	Finite set
$\mathbf{0}$	Zero matrix
$\mathbf{1}$	One matrix
$\mathbf{I}$	Identity matrix

Sets

$\mathbb{N}$	Natural numbers (excluding 0)
$\mathbb{R}$	Real numbers
$\mathbb{R}_+$	Real nonnegative numbers
$\mathbb{C}$	Complex numbers
$\mathbb{I}$	Probability domain $[0, 1]$
$\mathbb{H}_+^{n\times n}$	Positive semi-definite matrices of dimension $n \times n$
$\mathbb{U}^{n\times n}$	Unitary matrices of dimension $n \times n$

Operations

$(\cdot)^*$	Complex conjugate
$(\cdot)^\mathsf{T}$	Transpose
$(\cdot)^\mathsf{H}$	Hermitian (conjugate transpose)

$(\cdot)^{\dagger}$	Moore-Penrose inverse
$(\cdot)^{+}$	Ramp function $\max(0, \cdot)$
$\lvert\cdot\rvert$	Absolute value of a complex number
$\lVert\cdot\rVert$	Euclidean norm of a vector
$\lVert\cdot\rVert_{\mathrm{F}}$	Frobenius norm of a matrix
$\arg(\cdot)$	Argument of a complex number
$\mathrm{card}(\cdot)$	Cardinality of a finite set
$\log(\cdot)$	Natural logarithm of a real number
$\exp(\cdot)$	Exponential of a scalar or square matrix
$\mathrm{tr}(\cdot)$	Trace of a square matrix
$\det(\cdot)$	Determinant of a square matrix
$\mathrm{sv}(\cdot)$	Singular values sorted from largest to smallest
$\mathrm{diag}(\cdot)$	Constructs a square matrix with inputs on the main diagonal
$\mathrm{diag}^{-1}(\cdot)$	Retrieves the main diagonal of a square matrix
$\Re(\cdot)$	Retrieves the real part of a complex number
$\Im(\cdot)$	Retrieves the imaginary part of a complex number
$\mathbb{E}(\cdot)$	Expectation operator
$\mathbb{A}(\cdot)$	Extracts the Direct Current component of a signal
$\odot$	Hadamard product
$\otimes$	Kronecker product
$(\cdot)_{[x:y]}$	Shortcut for $(\cdot)_x, (\cdot)_{x+1}, \ldots, (\cdot)_y$

Distributions

$\sim$	Follows a distribution
$\mathcal{CN}(\mathbf{0}, \mathbf{\Sigma})$	Multivariate Circularly Symmetric Complex Gaussian with covariance $\mathbf{\Sigma}$

Subscripts

$(\cdot)_{\mathrm{B}}$	Backward
$(\cdot)_{\mathrm{D}}$	Direct
$(\cdot)_{\mathrm{F}}$	Forward
$(\cdot)_{\mathrm{I}}$	Information
$(\cdot)_{\mathrm{P}}$	Power

Superscripts

$(\cdot)^{(r)}$	r-th iterated value
$(\cdot)^{\star}$	Stationary point

Chapter 1

Introduction

1.1 Motivation

The quest for better wireless connectivity has been long-standing since Marconi's illuminating radio in 1895. Great successes have been made at the transmitter and receiver sides over the past century, and the communications society is unprecedentedly close to the Shannon limit [3]. By 2025, global mobile data traffic is expected to reach 607 exabytes per year [4] while the number of connected devices may exceed 75 billion [5]. At the same time, wireless applications are also evolving in various forms to address world-changing incidents like COVID-19, climate change, geopolitical tensions, and Artificial Intelligence (AI) revolution. An initial attempt was made in 5G where the network prioritizes among high-throughput, ubiquitous-coverage, high-reliability, low-latency, massive-connectivity, and energy-efficient services [6]. However, the desire of human and machine for better communication shows no signs of slowing down. Emerging applications such as smart cities, autonomous driving, telemedicine, extended reality, federated learning, and generative intelligence are calling for a stronger and smarter wireless infrastructure. It is envisioned that 6G will be designed to meet the following requirements [7–9]:

- *Throughput:* The network would be able to provide a peak data rate of 1 Tbps and an average data rate of 100 Gbps per user.
- *Latency:* Sub-millisecond end-to-end latency would be achieved for low-latency applications like autonomous driving and remote surgery.
- *Reliability:* A success rate of 99.9999% would be guaranteed for ultra-reliable applications like industrial automation and cooperative robotics.

- *Connectivity:* The number of connected devices per kilometer square would be increased to 10 million for supporting Internet of Everything (IoE).
- *Mobility:* Commercial airlines with a maximal velocity of 1000 km/h would be the target application scenario.
- *Energy efficiency:* Power consumption has been a major criticism for 5G. It is expected that energy per bit would be reduced by over 90% in 6G to reduce carbon footprints.
- *Positioning accuracy:* Thanks to THz base stations, a 3D positioning accuracy of centimeter level may be achieved for indoor and outdoor environments.
- *Coverage:* Poor coverage has been another bottleneck for 5G. A terrestrial-satellite-aerial integrated network would provide a ubiquitous and uniform coverage for urban, rural, and remote areas.
- *Security and privacy:* Physical-layer security can be improved with narrower beams at higher frequencies and destructive scattering at the environment. Privacy can be enhanced with federated learning and homomorphic encryption.

Beyond the statistical requirements above, the next-generation wireless network is desired to integrate human, machine, environment, and AI seamlessly for a harmonic ecosphere. This paradigm shift from *connectivity* to *intelligence* is fueled by the latest advances in machine learning (theory) and programmable metamaterials (hardware). The former enables the network to understand the environment while the latter evolves the environment from a chaotic medium to a conscious agent that can serve on demand. Together, they form a symbiotic relationship with the potential to revolutionize how the world energize, sense, communicate, and interact.

One promising candidate within this 6G vision is Reconfigurable Intelligent Surface (RIS), a programmable metasurface that recycles and redistributes the electromagnetic waves in the air for improved wireless performance. It could be incorporated into the transmitter and receiver for *beamforming*, employed as a free-rider information source for *modulation*, or simply placed in space as a standalone device for *channel shaping*. These applications have distinctive requirements and trade-offs, but the operation principles are the same and those roles are not mutually exclusive. Imagine a future where everything can be "smartened" by coating with a metamaterial layer and attaching a microcontroller tag. Only a few active radiating sources (like the sun) are needed, while most objects (like the universe) can exploit the surrounding waves to energize themselves, sense the environment, communicate with others, and help those in need when idle. This vision motivates three research questions to be addressed in this thesis:

- *How does RIS impact different wireless applications such as communication and far-field power transfer?*
- *Is it possible to integrate RIS with Backscatter Communication (BackCom) into a versatile tool that blurs the boundary between the network and environment?*
- *What is the ultimate limit of channel reshaping through passive RIS and what are the implications on transceiver designs?*

Before delving into these questions, we first provide a short overview of RIS and introduce some potential applications. A detailed literature review and technical discussion on RIS and other topics will be reserved for Chapter 2.

1.2 Overview on Reconfigurable Intelligent Surface (RIS)

1.2.1 Concept

RIS is commonly known as a planar surface involving numerous wave scattering elements (a.k.a. unit cells, reflective patches), whose amplitude and phase responses can be engineered in real-time to achieve a desired radiation pattern. It behaves like a delicate Radio-Frequency (RF) mirror with adjustable curvature and orientation, which allows the incident signals to be focused and redirected in a particular direction. As shown in Fig. 1.1, its typical architecture consists of three stacked layers and a controller [1]. The top layer is a two-dimensional array of scattering elements printed on a dielectric substrate. The elements directly interact with the impinging waves, which are usually fabricated from metamaterial or patch/dipole antennas with sub-wavelength dimension and spacing. The middle layer is a copper ground plate that provides voltage reference and avoids signal leakage. The bottom later is a circuit board that associate each element with adjustable components, such as varactor and Positive Intrinsic Negative (PIN) diodes [10]. It also hosts a Field-Programmable Gate Array (FPGA) controller that controls the circuit and coordinate with transceivers in the network. By adjusting the scatter response of all elements, the RIS can effectively manipulate the wavefront for a constructive or destructive superposition and thus improve the ambient wireless environment.

1.2.2 Characteristics

The key characteristics of RIS are summarized as follows:

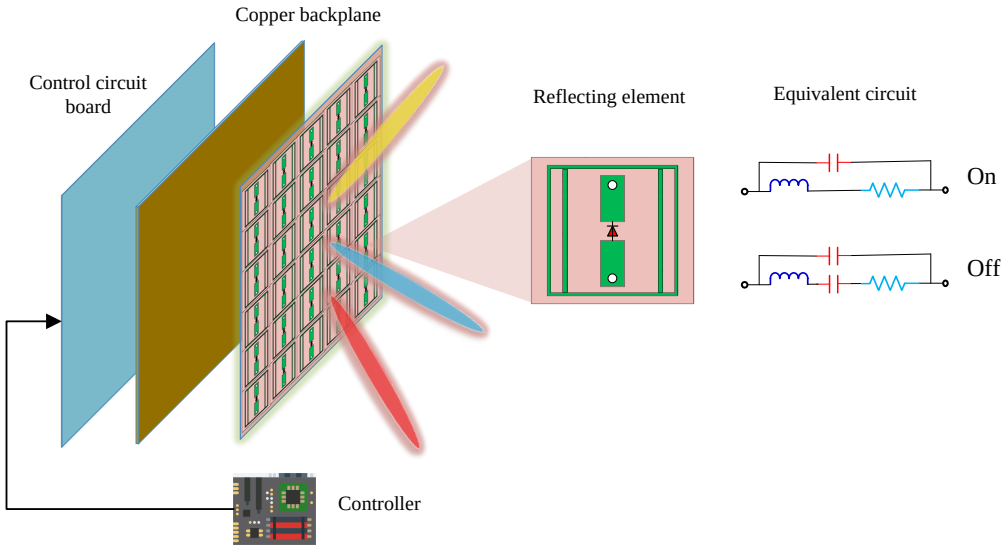

Fig. 1.1 A typical architecture of RIS. The figure is modified from [1].

- *Passive and environmental-friendly:* RIS reflects the incident waves in a passive manner and does not require dedicated RF chains.[1] This is different from Amplify-and-Forward (AF) relays that require power-hungry oscillators and introduces additional thermal noise.

- *Flexible:* It provides a software configurable environment that can be adapted for different applications and scenarios. This is different from conventional reflectarray [11] and frequency selective surfaces [12] with predefined radiation patterns and frequency response.

- *Full-duplex and universal:* This physical-layer solution can simultaneously support communication, sensing, and power transfer without self-interference. Thanks to channel reciprocity, the optimal configuration for downlink and uplink coincide with each other [13]. This is different from Decode-and-Forward (DF) relays that are designed for a specific communication link and suffers from packet delays.

- *Low-cost and conformal:* It can be manufactured from low-cost materials and deployed in various forms (e.g., walls, windows, ceilings, tables) to provide seamless coverage and powerful customization for indoor and outdoor environments. This is different from conventional multi-antenna systems that features complex hardware and bulky structures.

[1] The controller may be implemented with low-power components and powered by ambient energy.

1.2.3 Applications

The channel manipulation capability of RIS unlocks a wide range of unprecedented applications, such as signal enhancement [14], interference suppression [15], blockage bypassing [16], coverage extension [17], and security control [18]. It also has the potential to convey additional information [19], compensate for the Doppler effect [20], transform frequency-selective channels into frequency-flat [21], improve the spatial diversity for multi-antenna systems [22], and create artificial time diversity for multi-user orthogonal [23] and non-orthogonal [24] multiple accesses.

Those fancy characteristics and applications of RIS have also attracted significant attention from the industry. The first public testing attempt was made in 2018 by NTT Docomo and Metawave, which demonstrated a metasurface reflectarray in the FR2 band of 5G can boost a downlink data rate from $60\,\mathrm{Mbps}$ to $560\,\mathrm{Mbps}$ [25]. Later in 2020, NTT Docomo developed a transparent dynamic RIS that can allows 28GHz signals to reflect or pass through with negligible power loss. A regional "RIS alliance" was formed in 2021 by Chinese companies and institutes including ZTE, China Mobile, and CAICT, which soon released a white paper [26] to promote the technology and standardization. In December 2022, ITU-R drafted a recommendation report for IMT-2030 (6G) [27] that marks RIS as a key technology to enhance the radio interface for multiple physical dimension transmission. These developments showcase the rapid progress of RIS from theoretical concept to practical implementation, paving the way for its integration into the next-generation network.

1.3 Outline and Contributions

The thesis is outlined as follows:

- Chapter 1 provides an overview of the thesis. It introduces the motivation and objectives, discusses the characteristics and applications of RIS, and summarizes the topics and contributions of each research chapter. A list of publications is also provided.

- Chapter 2 provides the necessary background knowledge for the subsequent chapters, including the fundamental principles, hardware implementation, signal and system models, performance metrics, and design challenges for RIS, Wireless Power Transfer (WPT), Simultaneous Wireless Information and Power Transfer (SWIPT), BackCom, and Multiple-Input Multiple-Output (MIMO) systems. It also reviews the state-of-the-art research in relevant topics and raise critical questions to be addressed in the following chapters.

- Chapter **??** investigate the impact of RIS on wireless information and power transfer. The key contributions include:
  - Introduce RIS to a multi-antenna multi-carrier SWIPT system with different receiver architectures;
  - Consider joint waveform and beamforming design for the proposed system under a practical energy harvester model;
  - Characterize the Rate-Energy (R-E) performance trade-off by maximizing harvested energy subject to different communication rate constraints;
  - Propose local-optimal and low-complexity algorithms and evaluate their narrow and wideband performance through numerical simulations;
  - Discuss the array gain for communication and the scaling order for power transfer in terms of the number of transmit antennas and RIS elements.
- Chapter **??** develops a novel scatter protocol that integrates beamforming and modulation. The key contributions include:
  - Provide an in-depth comparison of RIS with state-of-the-art BackCom technologies and discuss the key properties of active and passive transmissions coexisting systems;
  - Unify RIS and BackCom as one battery-free cognitive radio called RIScatter, where dispersed or co-located scatter nodes ride over an active primary link to modulate their own information and engineering the legacy channel simultaneously;
  - Integrate backscatter modulation and passive beamforming seamlessly into the input distribution design that allows arbitrary trade-off in between;
  - Propose a low-complexity cooperative receiver that sequentially decodes both coexisting links and exploits backscatter detection as part of channel training;
  - Characterize the achievable primary-backscatter rate region over different designs of input distribution at the scatter nodes, active beamforming at the Access Point (AP), and energy detector at the receiver;
  - Discuss the impact of practical factors such as the number of scatter nodes and states, transmit antenna size, backscatter symbol duration, and Signal-to-Noise Ratio (SNR) on the system performance.
- Chapter **??** explores the ultimate channel shaping capabilities of RIS in MIMO systems. The key contributions include:

- Quantify the capability of a passive RIS to reshape the MIMO Point-to-point Channel (PC) in terms of singular values via analytical bounds and numerical optimization;
- Focus on a general Beyond-Diagonal (BD)-RIS architecture featuring element-wise connections and demonstrate its superior signal processing performance (subspace alignment and subchannel rearrangement) over the widely-adopted diagonal model;
- Propose an efficient Riemannian Conjugate Gradient (RCG) algorithm for general BD-RIS optimization and provide low-complexity solutions for quadratic problems;
- Characterize the Pareto frontiers of channel singular values and obtain power- and rate-optimal BD-RIS configurations in MIMO PC;
- Investigate the impact of BD-RIS on leakage interference suppression and Weighted Sum-Rate (WSR) maximization in MIMO Interference Channel (IC);
- Discuss how channel shaping helps to decouple joint RIS-transceiver designs with comparable performance and significantly reduced complexity.

1.4 Publications

- Y. Zhao, B. Clerckx, and Z. Feng, "IRS-aided SWIPT: Joint waveform, active and passive beamforming design under nonlinear harvester model," *IEEE Transactions on Communications*, vol. 70, pp. 1345–1359, 2022
- Y. Zhao and B. Clerckx, "Riscatter: Unifying backscatter communication and reconfigurable intelligent surface," 12 2022
- ——, *RIS in Wireless Information and Power Transfer*. John Wiley & Sons, Ltd, 2023, pp. 271–295
- Y. Zhao, H. Li, M. Franceschetti, and B. Clerckx, "Channel shaping using reconfigurable intelligent surfaces: From diagonal to beyond," *To be submitted to IEEE Transactions on Wireless Communications*

Chapter 2

Background and Literature Review

2.1 Reconfigurable Intelligent Surface (RIS)

2.1.1 Programmable Metamaterials

Metamaterials refer to artificial structures engineered for unusual properties that may not be found in nature. The concept was initially proposed by Victor Veselago in 1967, who conjectured the existence of mediums with negative dielectric constant $\epsilon < 0$ and negative permeability $\mu < 0$ [32]. Such metamaterials are known as "negative-index" because the refraction index is defined as the *negative* square root $n = -\sqrt{\epsilon\mu} < 0$, in order to be consistent with Maxwell's equations. It was not until 1999 that their feasibility was experimentally demonstrated by John Pendry at Imperial College using split-ring resonators [33]. Since then, metamaterials have attracted significant interests due to their counterintuitive properties, to name a few:

- *Negative refraction:* As shown in Fig. 2.1a, the incident and refracted rays stay at the same side of the normal axis [32]. This phenomenon is in contrast to the usual refraction but can still be predicted from Snell's law

$$\frac{\sin\theta_1}{\sin\theta_2} = n. \tag{2.1}$$

  It is worth mentioning that a generalized law of refraction and refraction has been proposed in [34], which has become a standard reference for the design and analysis of metamaterials.

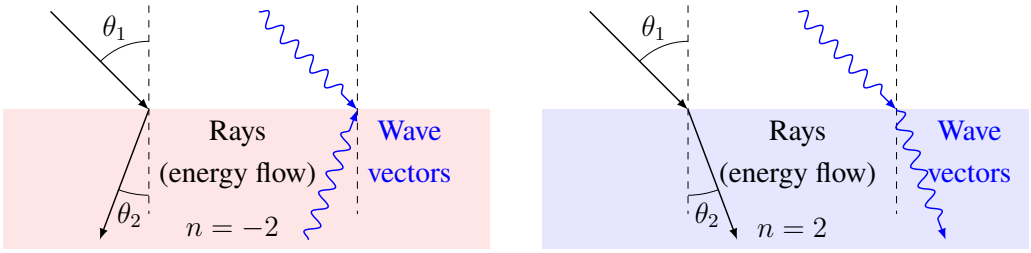

(a) Negative-Index Material (b) Positive-Index Material

Fig. 2.1 Refraction in negative and positive-index materials. Incident and refracted rays stay at the same side of the normal axis in a negative-index material.

- *Opposite wave direction:* As shown in Fig. 2.2a, the wave vector and energy flow (indicated by the Poynting vector) are opposite to each other in a negative-index material [35]. This can be inferred from the electric field equation

$$\vec{E} = \vec{E}_0 \exp(\jmath kz - \jmath \omega t) \tag{2.2}$$

where $k = k_0 n < 0$ is the wavenumber, $\vec{E}_0$ and k_0 are the free-space electric field and wavenumber reference, z is the propagation distance, ω is the angular frequency, and t is the time. Negative-index materials are thus also called "left-hand" because the propagation direction of the electric and magnetic fields can be determined by a left-hand rule.

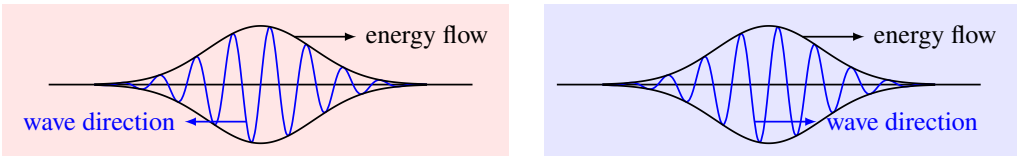

(a) Negative-Index Material (b) Positive-Index Material

Fig. 2.2 Wave and energy have opposite directions in a negative-index material.

Conventional metamaterials have fixed properties that depend on the geometry and arrangement of their constituent elements. Once fabricated, these properties cannot be easily changed unless the structure is physically altered. This limits their early usage to military and defense, with applications such as invisibility cloaks and optical illusions. In 2014, the concept of "coding" and "programmable" metamaterials was validated by researchers at Southeast University [36], who realized digital control of radar cross-section using biased diodes and FPGA. With a proper model of the target properties and external citation, the

metamaterial can be reconfigured in real-time for desired behaviors. For example, a self-adaptive metasurface equipped with motion and light sensors have been developed in [37] for single- and multi-beam steering.

Next, we discuss the principles of electromagnetic wave redirection via refraction and reflection:

- *Refraction:* As shown in Fig. 2.3a, the negative-index material can re-focus the beams diverging from a point source to another point behind the material [38]. This could be helpful for wireless applications where the transmitter and receiver are at different sides of the material.

- *Reflection:* As shown in Fig. 2.4b, the scattering elements cooperatively alter the phase of the incident wave for a constructive (or destructive) superposition of the reflected waves in the target direction [39]. This could be helpful for wireless applications where the transmitter and receiver are at the same side of the material.

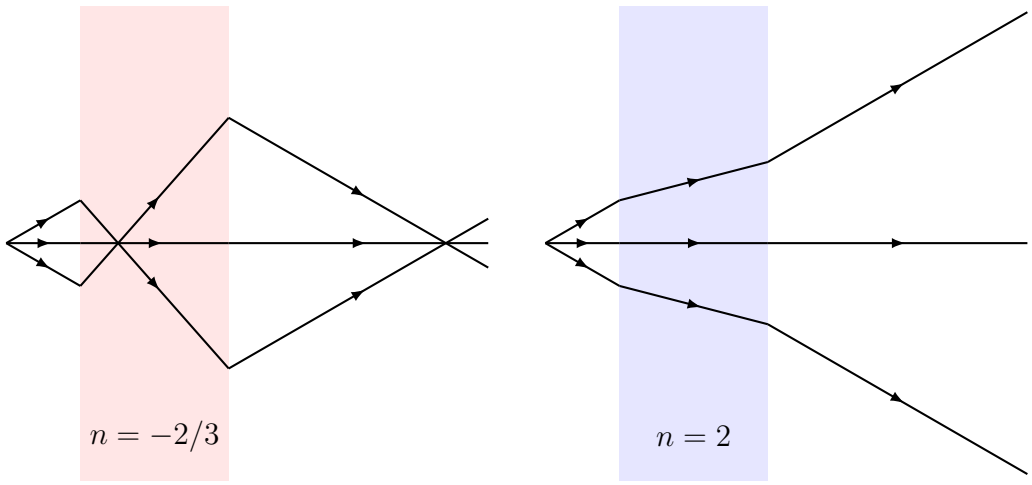

(a) Negative-Index Material (b) Positive-Index Material

Fig. 2.3 Refraction through metamaterials. For negative-index material, beams diverging from a point source is set in reverse and converges back to another point.

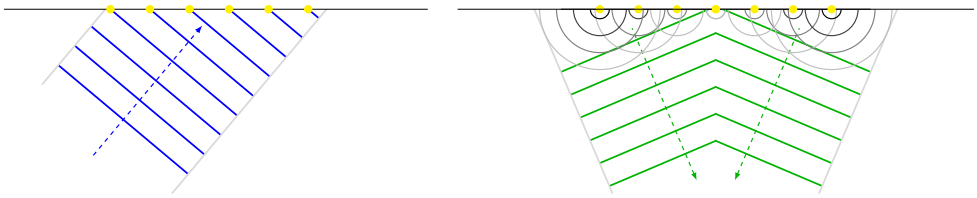

(a) Incident Wave (b) Reflected Wave

Fig. 2.4 Reflection through metamaterials. Yellow dots represent scattering elements. Solid and dashed lines denote wavefronts and rays, respectively. The scattering elements work together to manipulate the phases of incident waves, resulting in a focused beam steered in the intended direction.

It is worth noticing that refraction and reflection are different implementations of *passive beamforming* where the phase and amplitude of the ambient signal are altered by the metamaterial for a desired net effect. In the next subsection, we will some typical RIS scattering models and their physical architecture.

2.1.2 Wave Scattering Models

2.1.2.1 Principles

RF wave can be manipulated by scattering elements made from *programmable metamaterials* or *passive antennas* [40]. As discussed above, the former refracts or reflects the incident signals at the air-cell boundary and mainly applies a phase shift. In contrast, the latter allows the wave to feed into and collect from the antenna port such that some energy can be absorbed by the circuit and the rest is reradiated to the space. An interesting observation is that when excited by an external wave, a scattering element can simultaneously function as an object and a radiator. The corresponding scattered field is [41]

$$\vec{E}_{\text{scatter}}(Z_{\text{L}}) = \underbrace{\vec{E}_{\text{structural}}}_{\text{structural component}} + \underbrace{\Gamma I_{\text{M}} \vec{E}_{\text{antenna}}}_{\text{antenna component}}, \tag{2.3}$$

where Z_{L} is the load impedance, $\vec{E}_{\text{structural}}$ is the residual field under perfect matching (i.e., modelling as an object), $\vec{E}_{\text{antenna}}$ is the radiated field with unit current at the terminal and no external excitation (i.e., modelling as a radiator), I_{M} is the current under perfect matching, and Γ is the reflection coefficient

$$\Gamma = \frac{Z_{\text{L}} - Z_0^*}{Z_{\text{L}} + Z_0}, \tag{2.4}$$

and Z_0 is the characteristic impedance for programmable metamaterials or the input impedance for passive antennas. It is worth mentioning that

- *Structural component:* Depends on the geometry and material of the scatterer. It is usually modelled as part of the environment multipath [42, 43] or simply regarded a Direct Current (DC) offset when the impinging signal is Continuous Waveform (CW) [44].
- *Antenna component:* Depends on the reflection coefficient that can be altered by load impedance. This is widely exploited for various scattering applications, such as backscatter modulation in BackCom and passive beamforming in RIS [29].

We then introduce two canonical RIS models that will be adopted in the work chapters. More accurate models based on field equations (e.g., [45, 46]) and measurement fitting (e.g., [47]) are also available in the literature.

2.1.2.2 Diagonal Phase Shift Model

A straightforward way to model the RIS scattering effect is to consider independent scattering elements with purely reactive load impedance [48]. The reflection coefficient of the n-th element is thus

$$\theta_n = \frac{\jmath X_n - Z^*}{\jmath X_n + Z} = \exp(\jmath \phi_n), \tag{2.5}$$

where X_n is the reactance and ϕ_n is the phase shift on the scattered wave. For a total of N_{S} elements, the RIS scattering matrix is *diagonal with complex unit-magnitude entries*

$$\boldsymbol{\Theta} = \mathrm{diag}(\theta_1, \ldots, \theta_{N_{\mathrm{S}}}) = \begin{bmatrix} \theta_1 & 0 & \cdots & 0 \\ 0 & \theta_2 & \cdots & 0 \\ \vdots & \vdots & \ddots & \vdots \\ 0 & 0 & \cdots & \theta_{N_{\mathrm{S}}} \end{bmatrix}. \tag{2.6}$$

Despite the strong assumptions, this diagonal phase shift model is widely used for the analysis of RIS systems due to its simplicity and analytical tractability.

2.1.2.3 Beyond-Diagonal (BD) Model

How to model the RIS response if the passive scattering elements can be cooperative instead of independent? This question has been answered by [2] where a BD model was proposed. From a network theory perspective [49], the interaction between the scattering elements can be modelled as lossless (but not necessarily symmetric) in-group connections in an N_{S}-port

circuit network, as shown in Figs. 2.5 and 2.6 [2]. This architecture allows wave impinging on any element to propagate within the circuit and depart partially from other elements in the same group.

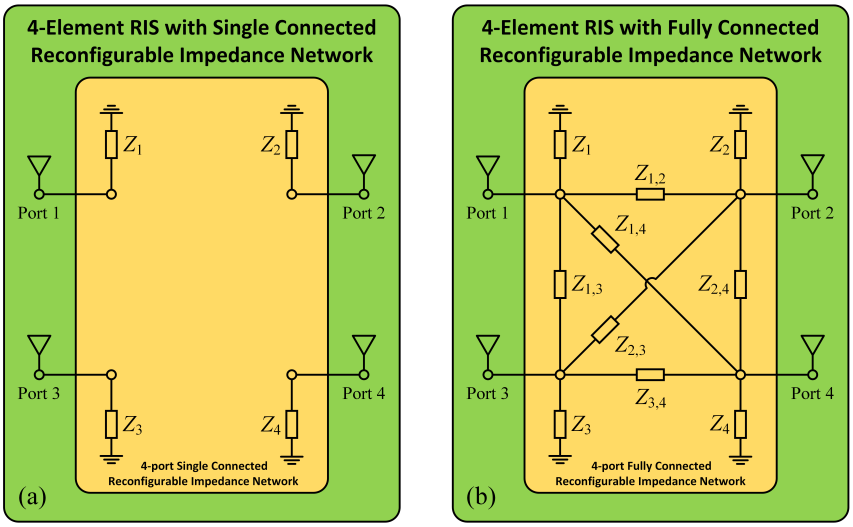

Fig. 2.5 Network model of a 4-element RIS with (a) independent scattering and (b) fully cooperative scattering with all elements interconnected. The figure is from [2].

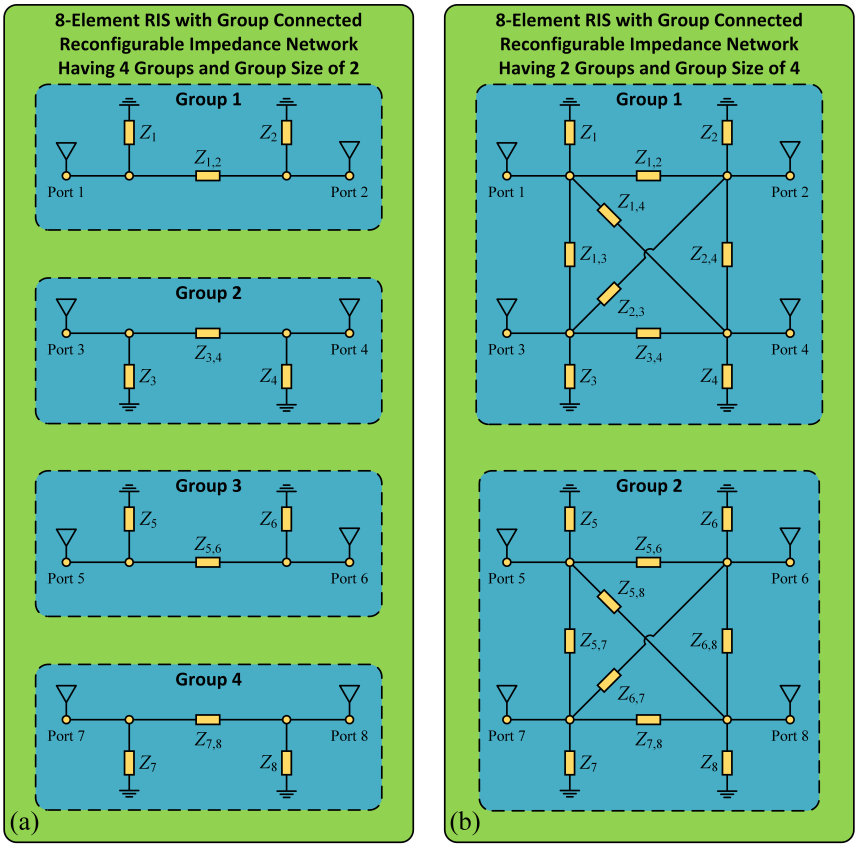

Fig. 2.6 Network model of an 8-element RIS with group-wise cooperative scattering of group size (a) 2 and (b) 4. The group size is a design parameter to balance the circuit complexity and scattering performance. The figure is from [2].

A general BD-RIS can be modeled as an N_{S}-port network that divides into G individual groups, each containing $L \triangleq N_{\mathrm{S}}/G$ elements interconnected by real-time reconfigurable connections. With symmetric components (e.g., capacitors and inductors), the scattering matrix of group $g \in \mathcal{G} \triangleq \{1, \ldots, G\}$ is [2]

$$\boldsymbol{\Theta}_g = (\jmath \mathbf{X}_g + Z_0 \mathbf{I})^{-1} (\jmath \mathbf{X}_g - Z_0 \mathbf{I}), \tag{2.7}$$

which satisfies both *symmetric* and *unitary* properties

$$\boldsymbol{\Theta}_g = \boldsymbol{\Theta}_g^{\mathsf{T}}, \tag{2.8a}$$

$$\boldsymbol{\Theta}_g^{\mathsf{H}} \boldsymbol{\Theta}_g = \mathbf{I}. \tag{2.8b}$$

On the other hand, lossless networks may also be built over asymmetric passive components (e.g., ring hybrids and branch-line hybrids) [50] such that the symmetric constraint (2.8a)

can be relaxed. This corresponds to the ultimate passive model where energy conservation (2.8b) is the only constraint for each group, as widely considered in quantum physics. The overall scattering matrix of asymmetric BD-RIS is thus *block-diagonal with unitary blocks*

$$\boldsymbol{\Theta} = \mathrm{diag}(\boldsymbol{\Theta}_1, \ldots, \boldsymbol{\Theta}_G) = \begin{bmatrix} \boldsymbol{\Theta}_1 & \mathbf{0} & \cdots & \mathbf{0} \\ \mathbf{0} & \boldsymbol{\Theta}_2 & \cdots & \mathbf{0} \\ \vdots & \vdots & \ddots & \vdots \\ \mathbf{0} & \mathbf{0} & \cdots & \boldsymbol{\Theta}_G \end{bmatrix}, \tag{2.9}$$

where (2.8b) is equivalently denoted as $\boldsymbol{\Theta}_g \in \mathbb{U}^{L\times L}$. The group size L is a design parameter to balance the circuit complexity and scattering performance. Diagonal (single-connected) and unitary (fully-connected) RIS can be viewed as extreme cases with group size $L = 1$ and $L = N_{\mathrm{S}}$, respectively. Therefore, the BD model (2.9) is envisioned to be the next-generation theoretical foundation for passive RIS, which grants more design freedom and stronger signal processing capability.

It is also worth mentioning that each group can be abstracted as a mathematical graph with L vertices and a variable number of edges [51]. One element is in the same group with another if and only if there is at least one path (via edges) between them. It implies that instead of connecting every pair of elements, the practical circuit can be designed to have a sparse graph with only a few connections, which is beneficial for reducing the circuit complexity and power loss from non-ideal components. Antenna directivity and radiation pattern should also be modelled in the scattering matrix, especially when the locations of users or RIS are not fixed. This has motivated the concept of Simultaneous Transmission and Reflection (STAR)-RIS [52, 53] and multi-sector RIS [54] where incident wave is partially steered to various directions for different users.

2.2 Wireless Power Transfer (WPT)

2.2.1 Introduction

Wireless devices are becoming smarter as well as more energy-efficient and eco-friendly. Koomey's law [55] predicts the computing efficiency roughly doubles every 19 months and the amount of power needed for the same operation decreases to 1% in a decade. Over the past 15 years, the rise of low-power technologies like Wireless Sensor Network (WSN) and Internet of Things (IoT) have hatched life-changing applications including smart homes, digital healthcare, and industrial automation. Today, Radio-Frequency Identification (RFID) tags and basic sensors (e.g., thermometer and proximeter) can operate on microwatts of power

[56, 57], while communication protocols like Bluetooth Low Energy (BLE) and Long Range Wide Area Network (LoRaWAN) only consume tens of milliwatts [58]. This low-power trend together with the upsurge of mobile devices is calling for a *truly wireless* energy solution that eliminates the need for periodic cable plugging or battery replacement. While great successes have been witnessed for candidates like solar and piezoelectric, their prospects in wireless systems remain unclear due to the bulky converter, unpredictable source, and limited operation range. One promising solution on the horizon is WPT through electromagnetic waves. It can be classified into two categories based on the operation principle [59]:

- *Non-radiative near-field:* Power is transferred over a short distance (typically a few centimeters) by inductive coupling between coils or capacitive coupling between electrodes in a field-to-field manner. The former has been widely standardized (e.g., Qi 2.0) and commercialized (e.g., wireless charging pads), while the latter is still in the research stage.

- *Radiative far-field:* Power is transferred over a long distance (typically a few meters) by directional microwave or laser beams between antennas in a point-to-point manner. It shares many similarities with RF communication (e.g., infrastructure and wireless environment) but suffers from lower energy efficiency than non-radiative WPT due to pathloss.

Radiative WPT[1] brings numerous opportunities to future wireless networks. First, it completely eliminates wired connections and can be integrated into existing wireless systems with minimum modifications. Those properties translate to simple deployment, high scalability, and low maintenance cost. Second, the power can be simultaneously radiated to multiple devices on demand in a predictable, sustainable and reliable manner. This supports our initial vision and is different from other uncontrollable and intermittent energy sources. Third and most importantly, radio waves carries power and information simultaneously. WPT can therefore be jointly designed with Wireless Information Transfer (WIT) to make the most of radiation, spectrum and infrastructures. However, energy efficiency and safety concerns have been two major obstacles that limit the practical development of WPT. In Section 2.3, we will discuss how RIS can help address these issues.

[1] In the following part of the thesis, WPT refers to radiative WPT.

2.2.2 Modules and Coupling Effect

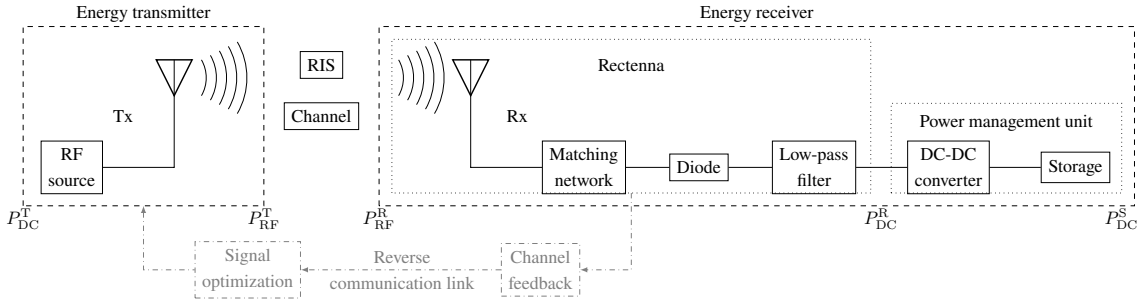

Fig. 2.7 Block diagram of a closed-loop RIS-aided WPT.

The block diagram a closed-loop RIS-aided WPT system is illustrated in Fig. 2.7. The RF signal is generated and radiated by the energy transmitter, propagated through a wireless channel in the presence of a RIS, captured by the antenna(s) at the receiver, converted to DC power by rectifier(s), then passed to the power management unit. Upon successful harvesting, the DC power is either delivered directly to the device or stored in a battery/super capacitor for future operations. When a feedback link is available, one can acquire Channel State Information (CSI) at the energy transmitter and exploit it for signal optimization. Such a closed-loop RIS-aided WPT system can provide a complete control of transmitter, channel, and receiver, which is essential for maximizing the end-to-end power transfer efficiency

$$\eta = \frac{P^{\mathrm{S}}_{\mathrm{DC}}}{P^{\mathrm{T}}_{\mathrm{DC}}} = \underbrace{\frac{P^{\mathrm{T}}_{\mathrm{RF}}}{P^{\mathrm{T}}_{\mathrm{DC}}}}_{\eta_1} \underbrace{\frac{P^{\mathrm{R}}_{\mathrm{RF}}}{P^{\mathrm{T}}_{\mathrm{RF}}}}_{\eta_2} \underbrace{\frac{P^{\mathrm{R}}_{\mathrm{DC}}}{P^{\mathrm{R}}_{\mathrm{RF}}}}_{\eta_3} \underbrace{\frac{P^{\mathrm{S}}_{\mathrm{DC}}}{P^{\mathrm{R}}_{\mathrm{DC}}}}_{\eta_4}, \tag{2.10}$$

where $P^{\mathrm{T}}_{\mathrm{DC}}$ is the transmitted DC power, $P^{\mathrm{T}}_{\mathrm{RF}}$ is the transmitted RF power, $P^{\mathrm{R}}_{\mathrm{RF}}$ is the received RF power, $P^{\mathrm{R}}_{\mathrm{DC}}$ is the received DC power, and $P^{\mathrm{S}}_{\mathrm{DC}}$ is the stored DC power. The power conversion efficiencies are specified below:

- η_1: Transmitter DC-to-RF conversion efficiency[2] that depends on the RF power amplifier and transmit antenna. It is also called "drain efficiency" and state-of-the-art designs can achieve $\eta_1 \geq 70\%$ [61].
- η_2: Channel RF-to-RF conversion efficiency that depends on the wireless environment and RIS configuration. This is the major bottleneck of WPT since the radiated power is inversely proportional to the propagation distance squared.

[2]This is different from Power-Added Efficiency (PAE) used in amplifier rating, which takes into account both DC power and input waveform power [60].

- η_3: Receiver RF-to-DC conversion efficiency that depends on the impedance matching and rectifier design. We will discuss its behavior and modelling in the next subsection.
- η_4: Storage DC-to-DC conversion efficiency that depends on the converter circuit and battery characteristics. Modern power management units can achieve a charging efficiency $\eta_4 \geq 90\%$ [62].

It is worth mentioning that η_1 and η_3 also depend on the characteristics of input waveform like power level, carrier frequency, and Peak-to-Average Power Ratio (PAPR) [63]. Extensive efforts have been contributed from RF, wireless communications, and power electronic communities to improve the conversion efficiency of individual modules. However, it is often overlooked in the literature that a practical WPT system is highly *non-linear* since the amplifier and rectifier are very sensitive to the input waveform. This non-linear behavior can lead to a *coupling effect* between the modules, such that optimizing η_1 to η_4 independently does not necessarily maximize the end-to-end power efficiency η [63]. Besides, the system modeling and analysis are subject to practical constraints like diode threshold and reverse-breakdown voltages, device parasitics, impedance mismatch, and harmonic generation [64].

2.2.3 Non-Linear Harvester Behavior

2.2.3.1 Equivalent Circuits

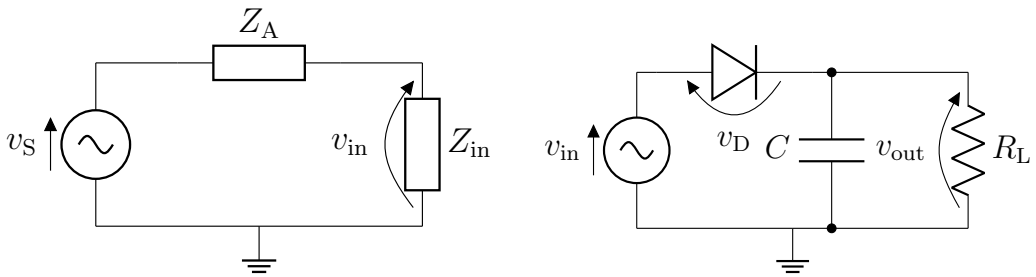

(a) Rectenna (b) Half-wave rectifier

Fig. 2.8 Equivalent circuit of (a) rectenna and (b) single-diode half-wave rectifier.

The rectifier is a nonlinear circuit that converts the RF signal to DC power by rectifying and filtering the input signal. Figs. 2.8 illustrates the equivalent circuits of a rectenna (antenna and rectifier) and a single-diode half-wave rectifier, where v_{S} is the source voltage on the receive antenna, $Z_{\mathrm{A}} = R_{\mathrm{A}} + \jmath X_{\mathrm{A}}$ is the antenna impedance, $Z_{\mathrm{in}} = R_{\mathrm{in}} + \jmath X_{\mathrm{in}}$ is the total impedance of the matching network and rectifier, v_{in} is input voltage on the matching network and rectifier, v_{D} is the diode voltage, C is the buffer capacitance, R_{L} is the rectifier

load resistance, and v_{out} is the output voltage. It is worth mentioning that the half-wave rectifier is the most popular choice in WPT literature due to its simple behavior and low cost. Other rectifier topologies like full-wave, bridge, and voltage doubler can potentially improve the RF-to-DC conversion efficiency [65], but their modeling and analysis are much more complicated.

2.2.3.2 Operation Regions and Signal Models

The diode is the key non-linear component that determines to the harvested energy. Generally speaking, the behavior of any rectenna can be separated into three operation regions [63]:

- *Linear region:* When the input power level is relatively low, the output power is proportional to the input and the RF-to-DC conversion efficiency η_3 is a constant. Most early WPT research (especially from communications society) assume the rectenna works in this region. For a received signal $y(t)$, the harvested DC power in this region can be modelled as
$$P_{\text{DC}}^{\text{R}} = \eta_3 P_{\text{RF}}^{\text{R}} = \eta_3 \mathbb{E}\big\{|y(t)|^2\big\}, \tag{2.11}$$
which suggests that maximizing the received RF signal power is sufficient to maximize the harvested DC power.

- *Non-linear (transition) region:* When the input power level is moderate, the output power increases *exponentially* with the input and η_3 is significantly higher than the linear region. This is the most interesting region that can be exploited to improve the overall power efficiency. For a tractable model, consider a perfectly matched ($Z_{\text{in}} = Z_{\text{A}}^*$) half-wave rectifier in Fig. 2.8(b) and assume the voltage across the matching network is negligible. The received RF power is totally transferred to the rectifier input $P_{\text{RF}}^{\text{R}} = \mathbb{E}\big\{|y(t)|^2\big\} = \mathbb{E}\big\{|v_{\text{in}}(t)|^2/R_{\text{in}}\big\} = \mathbb{E}\big\{|v_{\text{in}}(t)|^2/R_{\text{A}}\big\}$ such that the voltage sources can be expressed in terms of the received signal [63]
$$v_{\text{in}}(t) = y(t)\sqrt{R_{\text{A}}}, \quad v_{\text{S}}(t) = 2y(t)\sqrt{R_{\text{A}}}. \tag{2.12}$$
The current passing through the diode is given by the characteristic equation $i_{\text{D}}(t) = I_{\text{S}}\big(\exp(v_{\text{D}}(t)/nv_{\text{T}}) - 1\big)$, where I_{S} is the reverse bias saturation current, v_{T} is the thermal voltage, and n is the ideality factor. Its Taylor expansion around the steady point $-v_{\text{out}}$ is [63]
$$i_{\text{D}}(t) = \sum_{i=0}^{\infty} k_i \big(v_{\text{D}}(t) + v_{\text{out}}\big)^i = \sum_{i=0}^{\infty} k_i v_{\text{in}}^i(t) = \sum_{i=0}^{\infty} k_i R_{\text{A}}^{i/2} y^i(t), \tag{2.13}$$

where $k_0 = I_{\mathrm{S}}\big(\exp(-v_{\mathrm{out}}/nv_{\mathrm{T}}) - 1\big)$, $k_i = I_{\mathrm{S}}\frac{\exp(-v_{\mathrm{out}}/nv_{\mathrm{T}})}{i!(nv_{\mathrm{T}})^i}$ for $k \in \mathbb{N}$. The rectifier output DC current can be written as a function of the received signal

$$i_{\mathrm{out}} = \sum_{i=0}^{\infty} k_i R_{\mathrm{A}}^{i/2} \mathbb{E}\big\{y^i(t)\big\} = \sum_{i=0,\text{even}}^{\infty} k_i R_{\mathrm{A}}^{i/2} \mathbb{E}\big\{y^i(t)\big\} \tag{2.14}$$

where the second equality is because $\mathbb{E}\big\{y^i(t)\big\} = 0$ for odd i. Note that the dependency of k_i on $-v_{\mathrm{out}} = -i_{\mathrm{out}}R_{\mathrm{L}}$ makes it nontrivial to formulate a closed-form expression for the harvested DC power. Fortunately, it is shown in [63] that maximizing the harvested DC power is equivalent to maximizing the quantity

$$z = \sum_{i=2,\text{even}}^{\infty} \beta_i \mathbb{E}\big\{y^i(t)\big\}, \tag{2.15}$$

where $\beta_i = I_{\mathrm{S}}\frac{R_{\mathrm{A}}^{i/2}}{i!(nv_{\mathrm{T}})^i}$ is a constant. Truncating (2.15) at the second order yields the same result as (2.11), which suggests that the linear model is a special case of the more accurate non-linear model. For a moderate excitation, the contribution of higher-order terms is significant and should be modelled in the harvested DC power.

- *Saturation region:* When the input power level is too high, the diode works in the reverse breakdown region, the rectifier is saturated, and the output power is a constant. This is the region where the η_3 significantly drops and should be avoided by circuit design. For a fixed rectenna with Gaussian input signal, a parametric model was proposed in [66]

$$P_{\mathrm{DC}}^{\mathrm{R}} = \frac{\Psi_{\mathrm{DC}} - P_{\mathrm{sat}}\Omega}{1-\Omega}, \quad \Psi_{\mathrm{DC}} = \frac{P_{\mathrm{sat}}}{1+\exp\big(-a(P_{\mathrm{RF}}^{\mathrm{R}} - b)\big)}, \quad \Omega = \frac{1}{1+\exp(ab)}, \tag{2.16}$$

  where the constant P_{sat} denotes the maximum harvested power when the rectifier is saturated, and the constants a and b model the nonlinear charging rate with respect to input power and the minimum turn-on voltage of the rectifier, respectively. Parameters P_{sat}, a, and b can be obtained by curve fitting over measurement results.

The exact boundaries between those regions depend on the rectifier circuit and input waveform [67]. Signals with a higher PAPR usually exhibit the nonlinear and saturation effects at lower input power levels. For example, the nonlinear region is typically $[-20, 0]$ dBm for a CW and $[-30, -10]$ dBm for a multisine [68]. This not only motivates adaptive multi-carrier waveform designs [63, 67, 69, 70] but also calls for a joint optimization of the transmitter, channel (via RIS), and receiver to improve the end-to-end power efficiency.

2.3 Simultaneous Wireless Information and Power Transfer (SWIPT)

2.3.1 Rate-Energy (R-E) Tradeoff

2.3.2 Receiver Architectures

2.4 Backscatter Communication (BackCom)

2.4.1 Monostatic Backscatter Communication (MBC)

2.4.2 Bistatic Backscatter Communication (BBC)

2.4.3 Ambient Backscatter Communication (AmBC)

2.4.4 Symbiotic Radio (SR)

2.5 Multiple-Input Multiple-Output (MIMO)

2.5.1 Point-to-point Channel (PC): Channel Shaping

2.5.2 Interference Channel (IC): Interference Alignment

References

[1] Q. Wu and R. Zhang, "Towards smart and reconfigurable environment: Intelligent reflecting surface aided wireless network," *IEEE Communications Magazine*, vol. 58, pp. 106–112, 1 2020.

[2] S. Shen, B. Clerckx, and R. Murch, "Modeling and architecture design of reconfigurable intelligent surfaces using scattering parameter network analysis," *IEEE Transactions on Wireless Communications*, pp. 1–1, Nov. 2021.

[3] C. E. Shannon, "A mathematical theory of communication," *Bell System Technical Journal*, vol. 27, pp. 379–423, Jul 1948.

[4] F. Tariq, M. R. A. Khandaker, K.-K. Wong, M. A. Imran, M. Bennis, and M. Debbah, "A speculative study on 6g," *IEEE Wireless Communications*, vol. 27, pp. 118–125, 8 2020.

[5] D. Georgiev, "Internet of things statistics, facts & predictions [2024's update]," https://review42.com/resources/internet-of-things-stats/, accessed: 2024-03-13.

[6] M. Shafi, A. F. Molisch, P. J. Smith, T. Haustein, P. Zhu, P. D. Silva, F. Tufvesson, A. Benjebbour, and G. Wunder, "5g: A tutorial overview of standards, trials, challenges, deployment, and practice," *IEEE Journal on Selected Areas in Communications*, vol. 35, pp. 1201–1221, 6 2017.

[7] H. Tataria, M. Shafi, A. F. Molisch, M. Dohler, H. Sjoland, and F. Tufvesson, "6g wireless systems: Vision, requirements, challenges, insights, and opportunities," *Proceedings of the IEEE*, vol. 109, pp. 1166–1199, 7 2021.

[8] M. Alsabah, M. A. Naser, B. M. Mahmmod, S. H. Abdulhussain, M. R. Eissa, A. Al-Baidhani, N. K. Noordin, S. M. Sait, K. A. Al-Utaibi, and F. Hashim, "6g wireless communications networks: A comprehensive survey," *IEEE Access*, vol. 9, pp. 148 191–148 243, 2021.

[9] W. Jiang, B. Han, M. A. Habibi, and H. D. Schotten, "The road towards 6g: A comprehensive survey," *IEEE Open Journal of the Communications Society*, vol. 2, pp. 334–366, 2021.

[10] L. Dai, B. Wang, M. Wang, X. Yang, J. Tan, S. Bi, S. Xu, F. Yang, Z. Chen, M. D. Renzo, C.-B. Chae, and L. Hanzo, "Reconfigurable intelligent surface-based wireless communications: Antenna design, prototyping, and experimental results," *IEEE Access*, vol. 8, pp. 45 913–45 923, 2020.

[11] P. Nayeri, F. Yang, and A. Z. Elsherbeni, *Reflectarray Antennas: Theory, Designs, and Applications*. Wiley, 2 2018.

[12] R. Anwar, L. Mao, and H. Ning, "Frequency selective surfaces: A review," *Applied Sciences*, vol. 8, no. 9, p. 1689, Sep. 2018.

[13] Q. Wu, X. Zhou, and R. Schober, "IRS-assisted wireless powered NOMA: Do we really need different phase shifts in DL and UL?" *IEEE Wireless Communications Letters*, vol. 10, pp. 1493–1497, Jul 2021.

[14] Q. Wu and R. Zhang, "Intelligent reflecting surface enhanced wireless network via joint active and passive beamforming," *IEEE Transactions on Wireless Communications*, vol. 18, pp. 5394–5409, Nov 2019.

[15] T. Jiang and W. Yu, "Interference nulling using reconfigurable intelligent surface," *IEEE Journal on Selected Areas in Communications*, vol. 40, pp. 1392–1406, 5 2022.

[16] G. Ghatak, V. Malik, S. S. Kalamkar, and A. K. Gupta, "Where to deploy reconfigurable intelligent surfaces in the presence of blockages?" vol. 2021-September. IEEE, 9 2021, pp. 1419–1424.

[17] S. Zeng, H. Zhang, B. Di, Z. Han, and L. Song, "Reconfigurable intelligent surface (ris) assisted wireless coverage extension: Ris orientation and location optimization," *IEEE Communications Letters*, vol. 25, pp. 269–273, 1 2021.

[18] A. Almohamad, A. M. Tahir, A. Al-Kababji, H. M. Furqan, T. Khattab, M. O. Hasna, and H. Arslan, "Smart and secure wireless communications via reflecting intelligent surfaces: A short survey," *IEEE Open Journal of the Communications Society*, vol. 1, pp. 1442–1456, 2020.

[19] J. Ye, S. Guo, S. Dang, B. Shihada, and M.-S. Alouini, "On the capacity of reconfigurable intelligent surface assisted mimo symbiotic communications," *IEEE Transactions on Wireless Communications*, vol. 21, pp. 1943–1959, 3 2022.

[20] E. Basar, "Reconfigurable intelligent surfaces for doppler effect and multipath fading mitigation," *Frontiers in Communications and Networks*, vol. 2, 5 2021.

[21] E. Arslan, I. Yildirim, F. Kilinc, and E. Basar, "Over-the-air equalization with reconfigurable intelligent surfaces," *IET Communications*, vol. 16, pp. 1486–1497, 8 2022.

[22] O. Ozdogan, E. Bjornson, and E. G. Larsson, "Using intelligent reflecting surfaces for rank improvement in mimo communications." IEEE, 5 2020, pp. 9160–9164.

[23] Y. Yang, B. Zheng, S. Zhang, and R. Zhang, "Intelligent reflecting surface meets ofdm: Protocol design and rate maximization," *IEEE Transactions on Communications*, vol. 68, pp. 4522–4535, 7 2020.

[24] G. Chen and Q. Wu, "Fundamental limits of intelligent reflecting surface aided multiuser broadcast channel," *IEEE Transactions on Communications*, vol. 71, pp. 5904–5919, 10 2023.

[25] R. Liu, Q. Wu, M. D. Renzo, and Y. Yuan, "A path to smart radio environments: An industrial viewpoint on reconfigurable intelligent surfaces," *IEEE Wireless Communications*, vol. 29, pp. 202–208, 2 2022.

[26] R. Alliance, "Reconfigurable intelligent surface technology white paper," 2023.

[27] ITU-R, "Future technology trends of terrestrial international mobile telecommunications systems towards 2030 and beyond," Report ITU-R M.2516-0, 2022.

[28] Y. Zhao, B. Clerckx, and Z. Feng, "IRS-aided SWIPT: Joint waveform, active and passive beamforming design under nonlinear harvester model," *IEEE Transactions on Communications*, vol. 70, pp. 1345–1359, 2022.

[29] Y. Zhao and B. Clerckx, "Riscatter: Unifying backscatter communication and reconfigurable intelligent surface," 12 2022.

[30] ——, *RIS in Wireless Information and Power Transfer*. John Wiley & Sons, Ltd, 2023, pp. 271–295.

[31] Y. Zhao, H. Li, M. Franceschetti, and B. Clerckx, "Channel shaping using reconfigurable intelligent surfaces: From diagonal to beyond," *To be submitted to IEEE Transactions on Wireless Communications*.

[32] V. G. Veselago, "The electrodynamics of substances with negative ϵ and μ," *Soviet Physics Uspekhi*, vol. 10, pp. 509–514, 4 1968.

[33] J. Pendry, A. Holden, D. Robbins, and W. Stewart, "Magnetism from conductors and enhanced nonlinear phenomena," *IEEE Transactions on Microwave Theory and Techniques*, vol. 47, pp. 2075–2084, 1999.

[34] N. Yu, P. Genevet, M. A. Kats, F. Aieta, J.-P. Tetienne, F. Capasso, and Z. Gaburro, "Light propagation with phase discontinuities: Generalized laws of reflection and refraction," *Science*, vol. 334, pp. 333–337, 10 2011.

[35] J. Pendry, "Negative refraction," *Contemporary Physics*, vol. 45, pp. 191–202, 5 2004.

[36] T. J. Cui, M. Q. Qi, X. Wan, J. Zhao, and Q. Cheng, "Coding metamaterials, digital metamaterials and programmable metamaterials," *Light: Science & Applications*, vol. 3, no. 10, pp. e218–e218, Oct. 2014.

[37] Q. Ma, G. D. Bai, H. B. Jing, C. Yang, L. Li, and T. J. Cui, "Smart metasurface with self-adaptively reprogrammable functions," *Light: Science & Applications*, vol. 8, p. 98, 10 2019.

[38] W. J. Padilla, D. N. Basov, and D. R. Smith, "Negative refractive index metamaterials," *Materials Today*, vol. 9, pp. 28–35, 7 2006.

[39] M. Poulakis, "6g's metamaterials solution: There's plenty of bandwidth available if we use reconfigurable intelligent surfaces," *IEEE Spectrum*, vol. 59, pp. 40–45, 11 2022.

[40] Y. C. Liang, Q. Zhang, J. Wang, R. Long, H. Zhou, and G. Yang, "Backscatter communication assisted by reconfigurable intelligent surfaces," *Proceedings of the IEEE*, 2022.

[41] R. Hansen, "Relationships between antennas as scatterers and as radiators," *Proceedings of the IEEE*, vol. 77, pp. 659–662, May 1989.

[42] S. J. Thomas and M. S. Reynolds, "A 96 mbit/sec, 15.5 pj/bit 16-qam modulator for uhf backscatter communication." IEEE, Apr 2012, pp. 185–190.

[43] Y.-C. Liang, Q. Zhang, E. G. Larsson, and G. Y. Li, "Symbiotic radio: Cognitive backscattering communications for future wireless networks," *IEEE Transactions on Cognitive Communications and Networking*, vol. 6, pp. 1242–1255, Dec 2020.

[44] C. Boyer and S. Roy, "Backscatter communication and RFID: Coding, energy, and MIMO analysis," *IEEE Transactions on Communications*, vol. 62, pp. 770–785, Mar 2014.

[45] O. Ozdogan, E. Bjornson, and E. G. Larsson, "Intelligent reflecting surfaces: Physics, propagation, and pathloss modeling," *IEEE Wireless Communications Letters*, vol. 9, no. 5, pp. 581–585, May 2020.

[46] M. Najafi, V. Jamali, R. Schober, and H. V. Poor, "Physics-based modeling and scalable optimization of large intelligent reflecting surfaces," *IEEE Transactions on Communications*, vol. 69, pp. 2673–2691, 4 2021.

[47] S. Abeywickrama, R. Zhang, and C. Yuen, "Intelligent reflecting surface: Practical phase shift model and beamforming optimization," in *ICC 2020 - 2020 IEEE International Conference on Communications (ICC)*. IEEE, Jun. 2020, pp. 1–6.

[48] Q. Wu and R. Zhang, "Intelligent reflecting surface enhanced wireless network: Joint active and passive beamforming design," vol. 18. IEEE, Dec 2018, pp. 1–6.

[49] M. T. Ivrlac and J. A. Nossek, "Toward a circuit theory of communication," *IEEE Transactions on Circuits and Systems I: Regular Papers*, vol. 57, pp. 1663–1683, 7 2010.

[50] H.-R. Ahn, *Asymmetric Passive Components in Microwave Integrated Circuits*. Wiley, 2006.

[51] M. Nerini, S. Shen, H. Li, and B. Clerckx, "Beyond diagonal reconfigurable intelligent surfaces utilizing graph theory: Modeling, architecture design, and optimization," 5 2023.

[52] X. Mu, Y. Liu, L. Guo, J. Lin, and R. Schober, "Simultaneously transmitting and reflecting (star) ris aided wireless communications," *IEEE Transactions on Wireless Communications*, vol. 21, pp. 3083–3098, 5 2022.

[53] Y. Liu, X. Mu, J. Xu, R. Schober, Y. Hao, H. V. Poor, and L. Hanzo, "Star: Simultaneous transmission and reflection for 360° coverage by intelligent surfaces," *IEEE Wireless Communications*, vol. 28, pp. 102–109, 12 2021.

[54] H. Li, S. Shen, and B. Clerckx, "Beyond diagonal reconfigurable intelligent surfaces: A multi-sector mode enabling highly directional full-space wireless coverage," *IEEE Journal on Selected Areas in Communications*, vol. 41, pp. 2446–2460, 8 2023.

[55] J. Koomey, S. Berard, M. Sanchez, and H. Wong, "Implications of historical trends in the electrical efficiency of computing," *IEEE Annals of the History of Computing*, vol. 33, pp. 46–54, 3 2011.

[56] J. Huang, Y. Zhou, Z. Ning, and H. Gharavi, "Wireless power transfer and energy harvesting: Current status and future prospects," *IEEE Wireless Communications*, vol. 26, pp. 163–169, 8 2019.

[57] X. Hao, H. Zhang, Z. Shen, Z. Liu, L. Zhang, H. Jiang, J. Liu, and H. Liao, "A 43.2 μW 2.4 ghz 64-qam pseudo-backscatter modulator based on integrated directional coupler." IEEE, 5 2018, pp. 1–5.

[58] R. Correia and N. B. Carvalho, "Ultrafast backscatter modulator with low-power consumption and wireless power transmission capabilities," *IEEE Microwave and Wireless Components Letters*, vol. 27, pp. 1152–1154, 12 2017.

[59] J. Zhou, P. Zhang, J. Han, L. Li, and Y. Huang, "Metamaterials and metasurfaces for wireless power transfer and energy harvesting," *Proceedings of the IEEE*, vol. 110, pp. 31–55, 1 2022.

[60] J. Joung, C. K. Ho, K. Adachi, and S. Sun, "A survey on power-amplifier-centric techniques for spectrum- and energy-efficient wireless communications," *IEEE Communications Surveys & Tutorials*, vol. 17, pp. 315–333, 1 2015.

[61] A. Alizadeh, S. Hassanzadehyamchi, A. Medi, and S. Kiaei, "An x-band class-j power amplifier with active load modulation to boost drain efficiency," *IEEE Transactions on Circuits and Systems I: Regular Papers*, vol. 67, pp. 3364–3377, 10 2020.

[62] N. M. L. Tan, T. Abe, and H. Akagi, "Design and performance of a bidirectional isolated dc-dc converter for a battery energy storage system," *IEEE Transactions on Power Electronics*, vol. 27, pp. 1237–1248, 3 2012.

[63] B. Clerckx and E. Bayguzina, "Waveform design for wireless power transfer," *IEEE Transactions on Signal Processing*, vol. 64, no. 23, pp. 6313–6328, Dec. 2016.

[64] C. R. Valenta and G. D. Durgin, "Harvesting wireless power: Survey of energy-harvester conversion efficiency in far-field, wireless power transfer systems," *IEEE Microwave Magazine*, vol. 15, pp. 108–120, 6 2014.

[65] S. A. Rotenberg, S. K. Podilchak, P. D. H. Re, C. Mateo-Segura, G. Goussetis, and J. Lee, "Efficient rectifier for wireless power transmission systems," *IEEE Transactions on Microwave Theory and Techniques*, vol. 68, pp. 1921–1932, 5 2020.

[66] E. Boshkovska, D. W. K. Ng, N. Zlatanov, and R. Schober, "Practical non-linear energy harvesting model and resource allocation for swipt systems," *IEEE Communications Letters*, vol. 19, pp. 2082–2085, 12 2015.

[67] Y. Zeng, B. Clerckx, and R. Zhang, "Communications and signals design for wireless power transmission," *IEEE Transactions on Communications*, vol. 65, pp. 2264–2290, 5 2017.

[68] M. D. Prete, A. Costanzo, M. Magno, D. Masotti, and L. Benini, "Optimum excitations for a dual-band microwatt wake-up radio," *IEEE Transactions on Microwave Theory and Techniques*, vol. 64, pp. 4731–4739, 12 2016.

[69] Y. Huang and B. Clerckx, "Large-scale multiantenna multisine wireless power transfer," *IEEE Transactions on Signal Processing*, vol. 65, pp. 5812–5827, 11 2017.

[70] S. Shen and B. Clerckx, "Beamforming optimization for mimo wireless power transfer with nonlinear energy harvesting: Rf combining versus dc combining," *IEEE Transactions on Wireless Communications*, vol. 20, pp. 199–213, 1 2021.